**Atmospheric
Chemistry
and Physics
Discussions**

Iodine monoxide in the north subtropical free troposphere

O. Puentedura[1], M. Gil[1], A. Saiz-Lopez[2], T. Hay[2], M. Navarro-Comas[1], A. Gómez-Pelaez[3], E. Cuevas[3], and J. Iglesias[1]

[1]Instituto Nacional de Técnica Aeroespacial (INTA), Area de Investigación e Instrumentación Atmosférica, Ctra Ajalvir km4, 28850, Torrejón de Ardoz, Madrid, Spain
[2]Laboratory for Atmospheric and Climate Science, CSIC, Toledo, Spain
[3]Centro de Investigación Atmosférica de Izaña (Agencia Estatal de Meteorología – AEMET), Sta. Cruz de Tenerife, Spain

Correspondence to: O. Puentedura (puentero@inta.es)

Full Screen / Esc

Printer-friendly Version

Interactive Discussion

Abstract

Iodine monoxide (IO) was retrieved using a new multi-axis DOAS instrument deployed at the Izaña subtropical observatory as part of the Network for the Detection of Atmospheric Composition Change (NDACC) programme. The station is located
at 2370 m a.s.l., well above the trade wind inversion that limits the top of the marine boundary layer, and is hence representative of the free troposphere. We report daily observations from May to August 2010 at different viewing angles. During this period, the spectral signature of IO was unequivocally detected on every day of measurement. A mean IO differential slant column density (DSCD) of 1.2×10^{13} molecules cm^{-2} was
observed at 5° instrument elevation angle (IEA) on clear days using a single zenith reference for the reported period, with a day-to-day variability of 12 % at 1 standard deviation. At an IEA of 0°, the mean DSCD value for clear days is 2.0×10^{13} molecules cm^{-2}, with a day-to-day variability of 14 %. Based on simultaneous O_4 measurements, the IO mixing ratio is estimated to be 0.18 pptv in the free troposphere at an IEA of 5°.
Episodes of Saharan dust outbreaks were also observed, with large increases in the DSCDs at higher elevation angles, suggesting an enhancement of IO inside the dust cloud.

1 Introduction

UV-visible spectroscopy has, for decades, been used for stratospheric chemistry studies. In recent years, improvements in the Differential Optical Absorption Spectroscopy (DOAS) technique and advances in profile retrievals from Multi Axis-DOAS (MAX-DOAS) observation modes (Platt and Stutz, 2008) have made possible the detection of trace gases of tropospheric interest at very low concentrations. Among them, the detection of iodine monoxide (IO) in the marine boundary layer (MBL) has been reported by numerous studies (Alicke et al., 1999; Allan et al., 2000; Saiz-Lopez et al., 2007; Read et al., 2008). IO is involved in catalytic cycles of ozone loss in the MBL (e.g.

Chameides and Davis, 1980), reinforces the ozone depletion capacity of other halogen radicals such as BrO and intervenes in the releasing of Cl and Br from sea-salt (Vogt et al., 1999; McFiggans et al., 2000). Iodine chemistry has also been postulated to have an effect in modulating the ratios of OH/HO_2 and NO/NO_2 (e.g. Davis et al., 1996; Bloss et al., 2005) and in new particle formation at coastal sites that can potentially act as cloud condensation nuclei in the MBL (e.g. O'Dowd et al., 2002).

Measurements of tropospheric IO are mostly located in mid-latitude marine coastal areas such as Mace Head, Ireland (Alicke et al., 1999; Saiz-Lopez and Plane, 2004; Huang et al., 2010) and Roscoff, France (Peters et al., 2005; Wada et al., 2007; Whalley et al., 2007; Mahajan et al., 2009) where its detection is conditioned to the biogenic activity when some species of algae are exposed to the atmosphere, emitting mainly I_2 at low tide (Saiz-Lopez and Plane, 2004). Therefore, the concentrations of IO measured in these field campaigns are highly variable (between 1 and 9.8 pptv).

IO has also been measured under open ocean conditions, where local biogenic activity is supposed not to have an important impact. Observed concentrations are significantly lower than at coastal locations and with little annual variation (Mahajan et al., 2010). Observations performed during dedicated campaigns at Tenerife (Allan et al., 2000) and Cape Verde (Read et al., 2008) reported concentrations between 0.2 and 4 pptv.

IO has also been detected from space over high southern latitudes using the SCIA-MACHY instrument (Saiz-Lopez et al., 2007; Schöenhardt et al., 2008). However, at mid and low latitudes, IO signal-to-noise ratio is too low for SCIAMACHY retrievals, except over biologically active regions (Schöenhardt et al., 2008).

Recently, measurements using the MAX-DOAS technique from a ship cruise between Canary Islands and Cape Verde and the Mauritania coast during June 2010 (Grossmann et al., 2011) have shown very small amounts of IO close to the detection limit near the Tenerife Coast (0.8 pptv; 0.99×10^{13} molec cm^{-2}).

Field campaigns to detect IO have all been concentrated in the MBL whereas attempts to detect the molecule in the free troposphere (FT) are scarce. Butz et al. (2008)

reported an upper limit of 0.1 pptv at 13.5 km as measured by balloon-borne instrumentation using the solar occultation technique. Unfortunately, solar occultation does not allow observations of lower layers and the IO vertical distribution of IO within the troposphere still remains uncertain.

In this paper we report on the first observation of IO in the FT using MAX-DOAS at the Izaña observatory over three months of measurements from May 2010 to August 2010. Descriptions of the measurement site, the instrument, the DOAS retrieval and the radiative transfer model for calculation of box-air-mass factors (box-AMFs) are given in Sects. 2, 3 and 4 respectively. Results and discussion are then presented in Sects. 5 and 6.

2 Station description and meteorology

The Izaña Atmospheric Observatory is part of the Global Atmospheric Watch (GAW) programme and is managed by the CIAI (Centro de Investigación Atmosférica de Izaña) belonging to the Agencia Estatal de Meteorología (AEMET, Spain). It is located at 28°18′ N, 16°29′ W in Tenerife (the Canary Islands), 300 km from the African west coast at an altitude of 2370 m a.s.l. The Canary Islands are below the descending branch of the Hadley Cell, which favours a large scale high stability subsidence flow regime, resulting in a large number of clear-sky days per year and a quasi-permanent strong temperature inversion (trade wind inversion) established between 800 and 1500 m a.s.l. (Font, 1956; Milford et al., 2008) depending on time of day and season. A persistent sea of clouds at the inversion base is an almost permanent feature. This fact is due to the condensation resulting from up-forcing of the trade winds when encountering the north face of the Island and convection by surface solar heating transporting moisture and tracers vertically upwards. At any time of the year, the base of the inversion defining an upper limit to the MBL lies well below the level of the observatory, precluding pollution from the Sta. Cruz and Puerto de la Cruz coastal towns from reaching the station at night, except for occasions associated with the passing

of low pressure systems. During daytime, a valley-mountain breeze driven by Solar heating acts as a local mechanism to transport air from the well mixed MBL top up to the station level. Molecules such as CO_2, O_3 and H_2O can be considered as tracers since their concentration in the MBL and FT are very different. They are absorbed or
destroyed when ascending upslope. At noon, with upwelling air coming from lower layers, H_2O typically increases by 60 %, while O_3 and CO_2 decrease: 6.5 % (3 ppbv over 46 ppbv) and 0.25 % (1 ppmv in 389 ppmv) respectively. This breeze is superimposed on the synoptic wind which is dominant at the level of the station. The stronger the synoptic wind the lesser the influence of the upwelling breeze. Figure 1 shows a scheme
of the station profile. Trade winds, initially forced to ascend due to the orography, stop ascending and surround the island when they reach the inversion level.

3 Experimental

3.1 Instrument description

The RASAS-II MAX-DOAS spectrometer collects scattered radiation from the sky in
the 415–530 nm spectral interval. It is based on a Shamrok SR-163i spectrograph and a 1024×255 pixels DU420A-BU Andor Idus CCD camera. A circulating cryostat containing ethylene-glycol helped to keep the detector stabilized at the operation temperature of $-30\,°C$ in order to minimize dark current. Light enters the spectrograph through a fused silica round-to-line fibre bundle. The fibre end is 100 microns in width.
The diffraction grating is holographic with 1200 grooves mm^{-1} blazed at 300 nm.

The linear dispersion was 0.11 nm pixel^{-1}. The FWHM of the spectrograph in the selected spectral range ranged between 0.52 and 0.58 nm. An isolated housing, thermally controlled to $\pm 0.1\,°C$, minimized shifting and squeezing of the spectra due to thermal compression and expansion. Dry nitrogen was continuously pumped at 4 l min^{-1} to
prevent condensation on the detector. All critical parameters, such as detector temperature, humidity and housing temperature were recorded together with the atmospheric

spectra. The outer end of the fibre was connected to a black-painted tube and the Field Of View (FOV) was defined by a baffling structure. A quartz window at the fibre tip precludes the entry of dust or water. The entrance optics was attached to a motorized Pan-tilt unit (PTU-D47) manufactured by Direct Perception, enabling it to point

5 to any place of the sky. In-house software controlled the measurement regime, integration time, rejection of saturated spectra, motor movements and instrument ON/OFF switching. Note that the performance of the instrument has been tested in the CINDI semi-blind intercomparison campaign for MAX-DOAS NO_2 measurements during the Northern-Hemisphere summer of 2009 (Roscoe et al., 2010).

10 The RASAS-II spectrometer was installed on the terrace of the Izaña Observatory in March 2010 to complement zenith measurements carried out since 1993 under the framework of the NDACC. The outdoor optics of the instrument, located in the tower of the observatory, allowed measurements at negative elevation angles. In the present scheme, the lowest elevation was set to $-1°$ but elevations of $-6°$ are possible be-

15 fore the instrumental line of sight hits the ground. To minimise the effect of optical path changes due to solar azimuth variation, the instrument was pointed due north (azimuth $= 0°$) (Wittrock et al., 2004). Off-axis measurements were carried out continuously from 85° SZA in the morning to 85° SZA in the evening. At each elevation angle, spectra are accumulated for the time required for the Sun to move from 90° to 90.2°

20 SZA, which ranges from 60 to 90 s depending on the time of year. A complete cycle of elevations takes about 14 min.

3.2 IO retrieval

The analysis of spectra was performed using software developed at INTA based on the standard DOAS technique (Platt and Stutz, 2008). A detailed explanation of the

25 analysis routine can be found in Gil et al. (2008). IO was retrieved in the spectral interval from 417 to 440 nm, where three vibrational bands in the $A^2\prod_{3/2} \leftarrow X^2\prod_{3/2}$ electronic transition can be observed. Using this spectral range, interferences from O_4 are mostly avoided. In addition to IO (Gómez Martín et al., 2005), NO_2, O_3, O_4, Glyoxal

Title Page

Abstract | Introduction

Conclusions | References

Tables | Figures

◄◄ | ►►

◄ | ►

Back | Close

Full Screen / Esc

Printer-friendly Version

Interactive Discussion

and H_2O absorption cross-sections were included in the retrieval. A Raman scattering cross-section was generated by the WinDOAS package (Fayt and Van Roozendael, 2001) based on the algorithm described by Chance and Spurr (1997). Finally, the inverse of the reference spectrum was included as a pseudo-cross-section to account for stray light inside the spectrograph and detector residual dark current. Measurements were scheduled throughout daylight hours for selected elevation angles. The lowest Instrument Elevation Angle (IEA) was fixed to $-1°$. Zenith measurements were skipped around noon close to the summer solstice to avoid direct sun in the detector.

In order to reduce the spectral noise, a smoothing by using a 4-pixel boxcar filter has been applied to logarithm of the spectra and to cross-sections. Densities are reduced on average by 1 % as compared with non-smoothed spectra while RMS error is reduced by a factor of 0.67.

The settings are summarized in Table 1. The instrumental detection limit, computed as the absorption optical depths at the maximum differential absorption cross-section in the range that equals the residual RMS value (Schönhardt et al., 2008), is 5–8×10^{12} molec cm^{-2}. Figure 2 shows examples of IO spectral fits for a number of elevations in a given cycle.

4   Box-AMF calculations

In order to estimate the sensitivity of the measurements to the presence of IO in different altitude layers box-AMF calculations taking into account the instrumental FOV have been carried out.

The box-AMFs were determined using the NIMO full spherical Monte Carlo radiative transfer model (Hay, 2010). The model simulates backward photon trajectories from the instrument to the top of the atmosphere (TOA) using the Monte Carlo technique. The photon radiances are then determined for the different measurement geometries by weighting them by the extinction along adjoint trajectories between each scattering location and the TOA in the direction of the Sun.

The simulations were performed at SZA 40° with an opaque cloud layer at 1000 m a.s.l. with a cloud-top albedo of 0.8 (assumed cloud albedo below the station in the observation direction), and with no cloud and a sea surface albedo of 0.07. The aerosol profile used in the simulations had an extinction of 8×10^{-8} cm^{-1} at sea level, linearly decreasing to 0 cm^{-1} at 5000 m a.s.l., with an optical depth of 0.02 at 43 nm. Aerosol scattering has been treated using the Henyey-Greenstein parametrisation, with a single scattering albedo of 0.99 and an asymmetry parameter of 0.7.

5 Results and discussion

IO is observed on clear and clean days during the whole measurement period at all IEA. Upper panel in Fig. 3 shows hourly averaged IO DSCDs (4–10 measurements) for 70°, 5° and 0° elevation geometries for the whole period of observations as processed using a single reference on day number 180/2010 at morning 49° SZA.

The mean daily IO DSCD differences between the almost-zenith IEA of 70° and the horizon (in successive IO DSCD (0°–70°)) above the detection limit of the instrument are shown in Fig. 3 (middle panel).

Successive large Saharan intrusion events occurred during the reported period (Fig. 3, lower panel) as illustrated by the AOD obtained by the AERONET-CIMEL photometer installed in the station next to the spectrometer's outdoor optics.

Saharan dust outbreaks, extending vertically up to 6–7 km and AOD (500 nm) up to 1, are not exceptional. Under high dust loading, the difference between zenith sky and horizon IO DSCDs is reduced due to the increase of multiple scattering processes resulting in a highly diffused atmosphere, disturbing the measurements. Consequently, only clear and clean days, defined as AOD (500 nm) less than 0.05, are considered in the estimation of IO concentrations obtained at the observation site.

IO has been detected every clear day with a mean DSCD (0°–70°) value of 2.0×10^{13} molec cm^{-2}. The mean day-to-day variation at 1 standard deviation level was 14 % for the considered period.

Title Page

Abstract | Introduction

Conclusions | References

Tables | Figures

◀ | ▶

◀ | ▶

Back | Close

Full Screen / Esc

Printer-friendly Version

Interactive Discussion

Two autumn clear and clean days yielding low residuals have been selected as examples to illustrate the diurnal evolution of the IO DSCDs. The reason for choosing days out of the reported period is to have a continuous set of measurements from morning to evening, since around the summer solstice the instrument is switched off around noon to protect the detector from direct sun. In Fig. 4 the diurnal cycle of IO DSCD measurements is illustrated for 5 October (day 278) in panel (a), and 2 November (day 306) in panel (b). Minimum IO columns are observed around noon for elevation angles lower than 90° Generally larger values in the afternoon than in the morning are observed during the reported period.

O_4 retrieved in the 477 nm band for day 278 is shown to illustrate how smooth diurnal oscillations of the top of the MBL slightly perturb the horizontal paths (see Fig. 5a). The IO/O_4 ratio has been used to eliminate the variations in IO DSCD resulting from changes in the optical path. Results confirm that the noon minimum occurs at all elevations angles and is not associated with reductions in the optical path (see Fig. 5b). The temperature inversion level oscillates throughout the day due to heating/cooling of the surface. The vertical distance from the top-of-the-inversion (TI) to the station reaches a minimum around noon. If the IO amount observed at noon were related to the oscillation of the TI height, maximum values of IO would be expected instead of the minimum ones observed. Instead, IO decreases indicating a diurnal behaviour which is not directly related to vertical transport. A possible explanation for the IO minimum around noon is the reaction of $IO + HO_2$, an important reaction pathway at low IO concentrations, which at midday when HO_2 levels peak in the FT (Martinez et al., 2010) leads to the formation of a temporary iodine reservoir, HOI. However, the shape of the measured diurnal variation at Izaña is not characteristic of the known behavior of IO in the tropical MBL, since reported observations indicate a diurnal variation with a maximum at noon (Read et al., 2008).

During most of the time, the layer of clouds extending along the north face of Tenerife Island at the level of the inversion limits radiation from the MBL. Therefore, most of the upward radiation scattered to the instrument has previously been reflected from the

top of the clouds rather than from layers below the cloud or the low albedo ocean surface. However, due to the FOV used during the reporting period (6.5°), the arrival of a small amount of radiation from the MBL cannot be completely ruled out at the lowest elevation angles.

Figure 6a shows differential box AMF calculated for different observations geometries, considering a FOV of 6.5° and a cloud located below the observatory at 1000 m a.s.l. with an albedo of 0.8. The differential box-AMF indicates the sensitivity of the measurements to the presence of IO in different altitude layers. For IEA lower than 2°, the instrument is mostly sensitive to the layer at the observatory but some contribution to the observations from lower layers is still possible. However, the presence of a thick cloud layer located at the top of the MBL prevents radiation from lower levels from reaching the instrument.

The same exercise has been performed without considering a cloud (Fig. 7b). In this case the albedo has been set to 0.07. Although the maximum sensitivity of the instrument is still at the height of the observatory, the contribution of radiation from lower layers to the observations is higher than in the previous case. However, even if the model does not take into account a cloud, the sensitivity of observations to lower levels for IEA greater than 2° is lower than 7 %.

To ensure there is not a significant contribution from the MBL due to the wide FOV of the instrument, calculations of IO concentration have been performed using the data series at IEA 5°. Figure 3 top panel shows the IO DSCD (5°) as red triangles. In Fig. 3 (middle panel) the daily mean of DSCD (5°–70°), calculated taking into account DSCD above the detection limit, is shown in orange squares. The mean DSCD (5°–70°) value for pristine days is 1.2×10^{13} molec cm^{-2}. The mean day-to-day variation at 1σ was 12 % for the considered period.

The IO concentration can be estimated by a simple approximation based on the assumption that all extra absorption takes place along the segment of the line of sight when the instrument is pointing at 5°. Then,

$$[IO]=DSCD_{IO} \cdot [O_2]^2 / DSCD_{O_4}, \tag{1}$$

Title Page

Abstract | Introduction

Conclusions | References

Tables | Figures

◄ | ►

◄ | ►

Back | Close

Full Screen / Esc

Printer-friendly Version

Interactive Discussion

$DSCD_{IO}$ and $DSCD_{O_4}$ are directly measured and $[O_2]$ is obtained from the atmospheric pressure at the site: 770 hPa. For the mean DSCD value of 1.2×10^{13} molec cm^{-2} the estimated IO mixing ratio is 0.18 pptv.

To exclude the possibility of IO coming from MBL by upwelling, "in situ" water vapour measurements performed at Izaña have been taken into account. H_2O partial pressure holds a diurnal oscillation with maximum values around noon and minimum at night. Daily Marine Boundary Layer Penetration Index (MBLPI) can be defined as the area contained between the actual measurements and the straight line joining the H_2O partial pressure means of the preceding and the subsequent nights. The index takes into account the amplitude and the duration of the upwelling slope breeze. MBL concentrations of H_2O are larger than FT ones and the area is positive since H_2O increases during the day.

The results show that the breeze is far from being a steady and constant phenomenon, even in warm months (Fig. 7 (upper panel)) since it is largely dependent on the insolation and synoptic circulation. During Saharan events, when the Southern wind dominates, the breeze disappears. The lack of a clear correlation between the MBLPI and IO is not surprising since the width of the layer of ascending air is of tens to a few hundreds of meters (A. Gómez, personal communication, 2011) and the contribution to the signal in MAXDOAS measurements of optical paths near 40 km is very small.

In the absence of any other known processes exchanging air on a global scale between the MBL and FT we conclude that the observed IO in the FT represents an almost constant background in the subtropical open ocean FT, at least near the Canary archipelago. This work constitutes, to our knowledge, the first time that density columns of IO are reported in the FT.

As previously mentioned, multiple scattering enhancement occurring during Saharan dust events induces changes in the optical path. Figure 8 (upper panel) shows how, under these conditions zenith sky radiance increases strongly up to a factor of 3 at noon as compared to clean days. At the same time, the 0° elevation radiance decreases on

dusty days compared to clean days. The result is a quite uniform radiation distribution on the sky dome with little dependence on elevation angle (also observed by Wagner et al., 2002).

The O_2 dimer is a good proxy of the length of the optical path. Since the vertical oxygen distribution varies only slightly, changes in solar radiation absorption by O_4 have to be related to changes in path. Figure 8 (lower panel) shows an estimation of the differential path (in km) computed as the measured slant column divided by the concentration at the level of the station. Here the differential path is the difference between any path and the path corresponding to the reference spectrum at zenith. Figure 8 shows how a strong reduction in the path takes place in heavy Saharan aerosol conditions at lower elevation angles (0°) whereas at high angles (70°) almost no change is observed. Due to high aerosol loading, solar radiation is scattered closer to the instrument than on clear days. Under these conditions little difference between IO SCD (0°) and SCD (70°) is observed. Unidentified structures appear in the residuals of DOAS analysis, resulting in fitting errors larger than 50 % (from 2×10^{-4} to 3×10^{-4} RMS), thus increasing the uncertainties in the retrieved IO column.

The observed IO increases for the IEA 70° measurements during the Saharan events. As shown in Fig. 8, the zenith AMF suffers essentially no change. LIBRAD-TRAN Radiative transfer model exercises in multiple scattering, assuming an AOD (500 nm) equal to 1 above the station, agree with the observations. Calculations show that very little increase in the O_4 zenith AMF occurs when a dense aerosol layer is included. Thus, observed increases in the DSCDs must be due to larger IO concentrations in the FT. An IO enhanced airmass travelling inside the aerosol layer should be viewed in the zenith measurements when evaluated with a clear sky reference. In contrast, at 0° elevation, the enhancement is compensated by the strong decrease in the path resulting in a slight reduction of the DSCD.

Saharan dust events are associated with a change in wind direction from NW to S-SE 2–3 days before the arrival of the dust. The air temperature profile is modulated by the vertical dust distribution and the trade wind inversion is replaced by the inversion

Full Screen / Esc

Printer-friendly Version

Interactive Discussion

at the base of the dust cloud. Under these conditions, the composition of air reaching the station is dependent on the history of the airmass. O_3 presents concentrations inside the dust cloud to up of 50 % lower than on dust free conditions (Bonasoni et al., 2004). Williams et al. (2007) found clear enhancements in CH_3I concentrations by a factor ranging from 2 to 14 during dust events measurements carried out both at Izaña and at sea level. To explain their observations they considered a mechanism involving the stimulation of CH_3I production, either due to contact of dust aerosols with surface sea water and later transport to the observatory level or by contact with moist sea salt aerosols following dust coalescence. Similar to CH_3I, there is no delay between the arrival of the dust and the increase in IO in our observations. Although a connection between the enhancements of both species during severe Saharan outbreaks looks reasonable, the explanation of this possibility is beyond the scope of this work and further investigation is required to determine whether the increase of CH_3I in presence of low O_3 influences the IO concentration or if there are other mechanisms or IO precursors involved.

6 Conclusions

MAX-DOAS measurements from the subtropical station of Izaña starting on May 2010 show the presence of background levels of IO in the free troposphere, clearly above the inversion that delimits the MBL. IO has been observed every day of measurements, indicating that the presence of IO in the FT is not an occasional feature. The mean value of the IO DSCD between IEA 5° and vertical pointing scattered spectra for clean days during the reported measurement period is 1.2×10^{13} molec cm^{-2} with a day-to-day variation of 12 %. The diurnal variation on clear days shows a minimum at noon and slightly larger values in the afternoon than in the morning. Calculations based on an estimation of the optical path using O_4 measurements, give a mixing ratio of 0.18 pptv in the layer between the level of the observatory and 6 km a.s.l. The DSCD

(5°–70°) rather than the DSCD for lower elevation angles is used for this estimate in order to avoid any significant radiative contribution from the MBL due to the wide FOV of the instrument. The lack of correlation between IO SCD and upslope breeze diurnal wind, as well as the shape of IO diurnal variation strongly indicates that the levels of IO measured represent the background for the area, representative of the open ocean free troposphere.

Finally, systematic enhancements during Saharan dust events are observed supporting the previously proposed explanation of the existence of a mechanism that introduces significant amounts of IO precursors during such events at the station level.

References

Alicke, B., Hebestreit, K., Stuzt, J., and Platt, U.: Iodine oxide in the marine boundary layer, Nature, 387, 572–573, 1999.

Allan, B. J., McFiggans, G., and Plane, J.: Observations of iodine monoxide in the remote boundary layer, J.Geophys. Res., 105, 14363–14369, 2000.

Aschmann, J., Sinnhuber, B.-M., Atlas, E. L., and Schauffler, S. M.: Modeling the transport of very short-lived substances into the tropical upper troposphere and lower stratosphere, Atmos. Chem. Phys., 9, 9237–9247, doi:10.5194/acp-9-9237-2009, 2009.

Bloss, W. J., Lee, J. D., Jonson, G. P., Sommariva, R., Heard, D. E., Saiz-Lopez, A., Plane, J. M. C., McFiggans, G., Coe, H., Flynn, M., Williams, P., Richard, A. R., and Fleming, Z. L.:

Impact of halogen monoxide chemistry upon boundary layer OH and HO_2 concentrations at a coastal site, J. Res. Lett., 32, L06814, doi:10.1029/2004GL022084, 2005.

Bogumil, K., Orphal, J., Flaud, J.-M., and Burrows, J.-P.: Vibrational progressions in the visible and near ultraviolet absorption spectrum of ozone, Chem. Phys. Lett., 349, 241–248, 2001.

Bogumil, K., Orphal, J., Homann, T., Voigt, S., Spietz, P., Fleischmann, O. C., Vogel, A., Hartmann, M., Bovensmann, H., Frerick, J., and Burrows, J. P.: Measurements of molecular absorption spectra with the SCIAMACHY pre-fight model: Instrument characterization and reference data for atmospheric remote sensing in the 230–2380 nm region, J. Photoch. Photobio. A, 157, 167–184, 2003.

Bonasoni, P., Cristofanelli, P., Calzolari, F., Bonafè, U., Evangelisti, F., Stohl, A., Zauli Sajani, S., van Dingenen, R., Colombo, T., and Balkanski, Y.: Aerosol-ozone correlations during dust transport episodes, Atmos. Chem. Phys., 4, 1201–1215, doi:10.5194/acp-4-1201-2004, 2004.

Chameides, W. L. and Davis, D. D.: Iodine: Its possible role in tropospheric photochemistry, J.Geophys. Res., 85, 7383–7393, 1980.

Chance, K. V. and Spurr, R. J. D.: Ring effect studies: Rayleigh scattering, including molecular parameters for rotational Raman scattering, and the Fraunhofer spectrum, Appl. Optics, 36, 5224–5230, 1997.

Davis, D., Crawford, J., Liu, S., McKeen, S., Bandy, A., Thornton, D., Rowland, F., and Blake, D.: Potential impact of iodine on tropospheric levels of ozone and other critical oxidants, J.Geophys. Res., 101, 2135–2147, 1996.

Fayt, C. and Van Roozendael, M.: WinDOAS 2.1., User Manual, IASB-BIRA, 2001.

Font, I.: El Tiempo Atmosférico de las Islas Canarias, Servicio Meteorológico Nacional (INM), Serie A, No. 26, 1956.

Gil, M., Yela, M., Gunn, L. N., Richter, A., Alonso, I., Chipperfield, M. P., Cuevas, E., Iglesias, J., Navarro, M., Puentedura, O., and Rodríguez, S.: NO_2 climatology in the northern subtropical region: diurnal, seasonal and interannual variability, Atmos. Chem. Phys., 8, 1635–1648, doi:10.5194/acp-8-1635-2008, 2008.

Gómez Martín, J. C., Spietz, P., and Burrows, J. P.: Spectroscopic studies of the I_2/O_3 photochemistry Part 1: Determination of the absolute absorption cross sections of iodine oxides of atmospheric relevance, J. Photochem. Photobio. A, 176, 15–38, 2005.

Hay, T. D.: MAX-DOAS measurements of bromine explosion events in McMurdo Sound, Antarctica, Phd thesis, University of Canterbury, 2010.

Iodine monoxide in the north subtropical free troposphere

O. Puentedura et al.

Title Page

Abstract	Introduction
Conclusions	References
Tables	Figures

|◀| |▶|
|◀| |▶|

Back | Close

Full Screen / Esc

Printer-friendly Version

Interactive Discussion

Huang, R.-J., Seitz, K., Buxmann, J., Pöhler, D., Hornsby, K. E., Carpenter, L. J., Platt, U., and Hoffmann, T.: In situ measurements of molecular iodine in the marine boundary layer: the link to macroalgae and the implications for O_3, IO, OIO and NO_x, Atmos. Chem. Phys., 10, 4823–4833, doi:10.5194/acp-10-4823-2010, 2010.

5   Mahajan, A. S., Oetjen, H., Saiz-Lopez, A., Lee, J. D., McFiggans, G. B., and Plane, J. M. C.: Reactive iodine species in a semi-polluted environment, Geophys. Res. Lett., 36, L16803, doi:10.1029/2009GL038018, 2009.

Mahajan, A. S., Plane, J. M. C., Oetjen, H., Mendes, L., Saunders, R. W., Saiz-Lopez, A., Jones, C. E., Carpenter, L. J., and McFiggans, G. B.: Measurement and modelling of tropo-

10   spheric reactive halogen species over the tropical Atlantic Ocean, Atmos. Chem. Phys., 10, 4611–4624, doi:10.5194/acp-10-4611-2010, 2010.

Martinez, M., Harder, H., Kubistin, D., Rudolf, M., Bozem, H., Eerdekens, G., Fischer, H., Klüpfel, T., Gurk, C., Königstedt, R., Parchatka, U., Schiller, C. L., Stickler, A., Williams, J., and Lelieveld, J.: Hydroxyl radicals in the tropical troposphere over the Suriname rainforest:

15   airborne measurements, Atmos. Chem. Phys., 10, 3759–3773, doi:10.5194/acp-10-3759-2010, 2010.

McFiggans, G., Plane, M. C., Allan, B. J., Carpenter, L., Coe, H., and O'Dowd, C.: A modelling study of iodine chemistry in the marine boundary layer, J. Geophys. Res., 105, 14371–14385, 2000.

20   McFiggans, G., Bale, C. S. E., Ball, S. M., Beames, J. M., Bloss, W. J., Carpenter, L. J., Dorsey, J., Dunk, R., Flynn, M. J., Furneaux, K. L., Gallagher, M. W., Heard, D. E., Hollingsworth, A. M., Hornsby, K., Ingham, T., Jones, C. E., Jones, R. L., Kramer, L. J., Langridge, J. M., Leblanc, C., LeCrane, J.-P., Lee, J. D., Leigh, R. J., Longley, I., Mahajan, A. S., Monks, P. S., Oetjen, H., Orr-Ewing, A. J., Plane, J. M. C., Potin, P., Shillings, A. J. L., Thomas, F., von

25   Glasow, R., Wada, R., Whalley, L. K., and Whitehead, J. D.: Iodine-mediated coastal particle formation: an overview of the Reactive Halogens in the Marine Boundary Layer (RHaMBLe) Roscoff coastal study, Atmos. Chem. Phys., 10, 2975–2999, doi:10.5194/acp-10-2975-2010, 2010.

Milford, C., Marrero, C., Martin, C., Bustos, J. J., and Querol, X.: Forecasting the air pollution

30   episode potential in the Canary Islands, Adv. Sci. Res., 2, 21–26, doi:10.5194/asr-2-21-2008, 2008.

O'Dowd, C. D., Hämeri, K., Mäkelä, J. M., Pirjola, L., Kulmala, M., Jennings, S. G., Berresheim, H., Hansonn, H.-C., de Leeuw, G., Kunx, G. J., Allen, A. G., Hewitt, C. N., Jackson, A.,

Iodine monoxide in the north subtropical free troposphere

O. Puentedura et al.

Title Page

Abstract | Introduction

Conclusions | References

Tables | Figures

◄ | ►►

◄ | ►

Back | Close

Full Screen / Esc

Printer-friendly Version

Interactive Discussion

Viisanen, Y., and Hoffmann, T.: J. Geophys. Res., 107, 8108, doi:10.1029/2001JD000555, 2002.

Platt, U. and Stutz, J.: Differential Optical Absorption Spectroscopy: Principles and Applications, Springer-Verlag, Berlin, Germany, 2008.

Peters, C., Pechtl, S., Stutz, J., Hebestreit, K., Hnninger, G., Heumann, K. G., Schwarz, A., Winterlik, J., and Platt, U.: Reactive and organic halogen species in three different European coastal environments, Atmos. Chem. Phys., 5, 3357–3375, doi:10.5194/acp-5-3357-2005, 2005.

Read, K. A., Mahajan, A. A., Carpenter, L. C., Evans M. J., Faria, B. V., Heard, D. E., Hopkins, J. R., Lee, J. D., Moller, S., Lewis, A. C., Mendes, L., McQuaid, J. B., Oetjen, H., Saiz-Lopez, A., Pilling, M. J., and Plane, J. M. C.: Extensive halogen-mediated ozone destruction over the sub-tropical Atlantic Ocean, Nature, 453, 1232–1235, 2008.

Rodgers, R. C.: Inverse methods for atmospheric soundings: Theory and practise, World Scientific Publishing, 2000.

Rothman, L. S., Gordon, I. E., Barbe, A., Benner, D. C., Bernath, P. F., Birk, M., Boudon, V., Brown, R., Campargue, A., Champion, J.-P., Chance, V., Coudert, L. H., Dana, V., Devi, V. M., Sally, S., Flaud, J.-M., Gamache, R. R., Goldman, A., Jacquemart, D., Kleiner, I., Lacome, N., Lafferty, W. J., Mandin, J.-Y., Massie, S. T., Mikhailenko, S. N., Miller, C. E., Moazzen-Ahmadi, N., Naumenko, O. V., Nikitin, A. V., Orphal, J., Perevalov, V. I., Perrin, A., Predoi-Cross, A., Rinsland, C. P., Rotger, M., Simeckova, M., Smith, M. A. H., Sung, K., Tashkun, S. A., Tennyson J., Toth, R. A., Vandaele, A. C, Vander Auwera, J.: The HITRAN 2008 molecular spectroscopic database, J. Quant. Spectrosc. Ra., 110, 533–572, 2009.

Roscoe, H. K., Van Roozendael, M., Fayt, C., du Piesanie, A., Abuhassan, N., Adams, C., Akrami, M., Cede, A., Chong, J., Clémer, K., Friess, U., Gil Ojeda, M., Goutail, F., Graves, R., Griesfeller, A., Grossmann, K., Hemerijckx, G., Hendrick, F., Herman, J., Hermans, C., Irie, H., Johnston, P. V., Kanaya, Y., Kreher, K., Leigh, R., Merlaud, A., Mount, G. H., Navarro, M., Oetjen, H., Pazmino, A., Perez-Camacho, M., Peters, E., Pinardi, G., Puentedura, O., Richter, A., Schönhardt, A., Shaiganfar, R., Spinei, E., Strong, K., Takashima, H., Vlemmix, T., Vrekoussis, M., Wagner, T., Wittrock, F., Yela, M., Yilmaz, S., Boersma, F., Hains, J., Kroon, M., Piters, A., and Kim, Y. J.: Intercomparison of slant column measurements of NO$_2$ and O$_4$ by MAX-DOAS and zenith-sky UV and visible spectrometers, Atmos. Meas. Tech., 3, 1629–1646, doi:10.5194/amt-3-1629-2010, 2010.

Saiz-Lopez, A. and Plane, J. M. C.: Novel iodine chemistry in the marine boundary layer,

Geophys. Res. Lett., 31, L04112, doi:10.1029/2003GL019215, 2004.

Saiz-Lopez, A., Mahajan, A. S., Salmon, R. A, Bauguitte, S., Jones, A. E., Roscoe, H. K., and Plane, J. M. C.: Boundary layer halogens in coastal Antarctica, Science, 317, 348–351, 2007a.

Saiz-Lopez, A., Chance, K., Liu, X., Kurosu, T. P., and Sander, S. P.: First Observation of Iodine Oxide from Space, Geophys. Res. Lett., 34, L12812, doi:1029/2007GL030111, 2007b.

Schönhardt, A., Richter, A., Wittrock, F., Kirk, H., Oetjen, H., Roscoe, H. K., and Burrows, J. P.: Observations of iodine monoxide columns from satellite, Atmos. Chem. Phys., 8, 637–653, doi:10.5194/acp-8-637-2008, 2008.

Vandaele, A. C., Hermans, C., Simon, P. C., Carleer, M., Colins, R., Fally, S., Mérienne, M. F., Jenouvrier, A., and Coquart, B.: Measurements of the NO_2 Absorption Cross-Sections from $42000\,cm^{-1}$ to $10000\,cm^{-1}$ (238–1000 nm) at 220 K and 294 K, J. Quant. Spectrosc. Ra., 59, 171–184, doi:10.1016/S0022-4073(97)00168-4, 1998.

Vogt, R., Sander, R., Von Glasow, R., and Crutzen, P.,J.: Iodine Chemistry and its Role in Halogen Activation and Ozone Loss in the Marine Boundary Layer: A Model Study, J. Atmos. Chem., 32, 375–395, doi:10.1023/A:1006179901037, 1999.

Volkamer, R., Spietz, P., Burrows, J., and Platt, U.: High-resolution Absorption Cross-Section of Glyoxal in the UV/Vis and IR Spectral Ranges, J. Photochem. Photobio. A, 172, 35–46, doi:10.1016/j.jphotochem.2004.11.011, 2005.

Wada, R., Beames, J. M., and Orr-Ewing, A. J.: Measurement of IO radical concentrations in the marine boundary layer using a cavity ring-down spectrometer, J.Atmos. Chem., 58, 69–87, doi:10.1007/s10874-007-9080-z, 2009.

Wagner, T., Dix, B., v. Friedeburg, C., Friess, U., Sinreich, R., and Platt, U.: MAX-DOAS O4 measurements: A new technique to derive information on atmospheric aerosols – Principles and information content, J. Geophys. Res., 109, D22205, doi:10-1029/2004JD0044904, 2004.

Whalley, L. K., Furneaux, K. L., Gravestock, T., Atkinson, H. M., Bale, C. S. E., Ingham, T., Bloss, W. J., and Heard, D. E.: Detection of Iodine Monoxide Radicals in the Marine Boundary Layer using Laser Induced Fluorescence Spectroscopy, J. Atmos. Chem., 58, 19–39, 2007.

Williams, J., Gros, V., Atlas, E., Maciejczyk, K., Batasaikhan, H., Schöler, H. F., Forster, C., Quack, B., Yassaa, N., and Van Digenen, R.: Possible Evidence for a Connection between Methyl Iodide Emissions and Saharan Dust, J. Geophys. Res., 112, D07303,

doi:1029/2005JD006702, 2007.

Wittrock, F., Oetjen, H., Richter, A., Fietkau, S., Medeke, T., Rozanov, A., and Burrows, J. P.: MAX-DOAS measurements of atmospheric trace gases in Ny-Ålesund – Radiative transfer studies and their application, Atmos. Chem. Phys., 4, 955–966, doi:10.5194/acp-4-955-2004, 2004.

Iodine monoxide in the north subtropical free troposphere

O. Puentedura et al.

Title Page

Abstract | Introduction

Conclusions | References

Tables | Figures

|◄ | ►|

◄ | ►

Back | Close

Full Screen / Esc

Printer-friendly Version

Interactive Discussion

Table 1. Instrumental and analysis settings for IO retrieval.

Instrumental	
F.O.V.	6.5°
Instrument Elevation Angles (IEA)	90°, 70°, 30°, 10°, 5°, 3°, 2°, 1°, 0°, −1°
Azimuth	Fixed to North
Time for collecting a single spectrum	From 0.2 s at noon to 10 s at 90° SZA
Time for a single measurement	Spectra co-added for ≈ 1 min
Time of a complete cycle	14 min

Fit parameters	
Spectral interval	417–440 nm
Orthogonalization Polynomial	3rd degree
Smoothing	4-pixels Boxcar
Offset	Inverse of the reference
Reference spectrum	A single one for all period. At zenith and sza = 50°

Absorption Cross-sections

Molecule	Temperature	Reference
O_3 (Io = 10^{19} molec cm^{-2})	223 K and 243 K	Bogumil et al. (2000)
NO_2 ($I_0 = 5 \times 10^{16}$ molec cm^{-2})	220 K and 298 K	Vandaele et al. (2002)
O_4	298 K	Greenblatt et al. (1990)
IO	298 K	Gómez Martín et al. (2005)
H_2O	298 K	Rothman et al. (2009)
Glyoxal	296 K	Volkamer et al. (2004)
Rot. Raman Scatt. (Ring effect)		WINDOAS package
		Fayt and Van Roozendael (2001)

Full Screen / Esc

Printer-friendly Version

Interactive Discussion
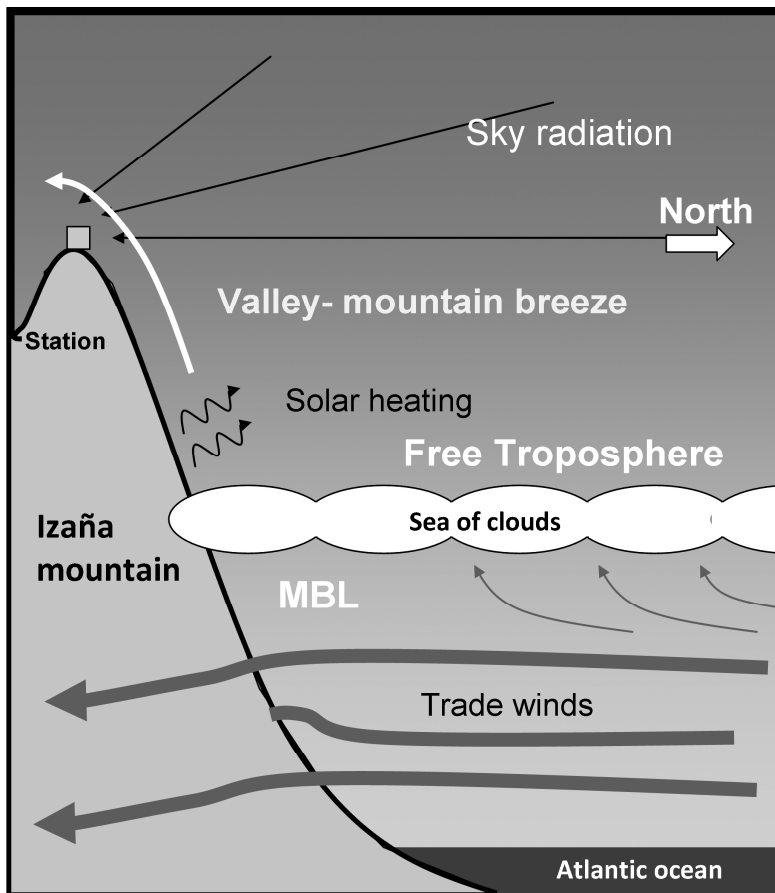
Fig. 1. Schematic view of the Izaña station from the North face. The sea of clouds drifts between 800 m in summer months to 1500 m in winter months.

Fig. 2. Detected IO absorption structures for a number of elevation angles on day 180 at SZA = 70° pm.
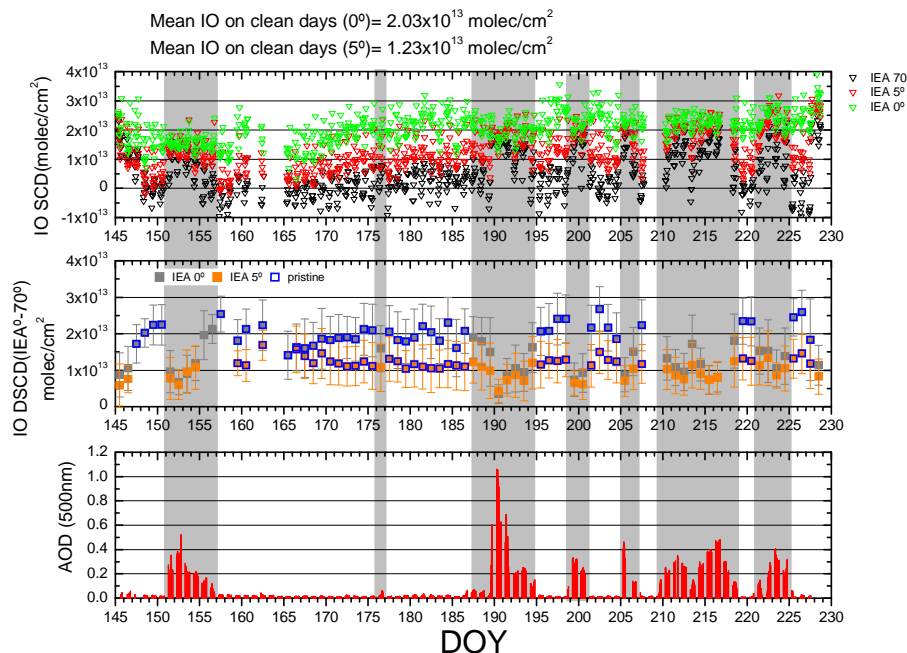
Fig. 3. Evolution of the hourly averaged IO DSCD for 0°, 5° and 70° elevation angles (upper plot) and daily mean differences of DSCD (middle plot). Clear days with no Saharan dust contribution are shown in hollow blue. Error bars represent the standard deviation of the diurnal mean. Aerosol Optical Depth (AOD) at 550 nm is displayed in the bottom plot. Grey shadowed areas denote days when AOD are larger than 0.05.
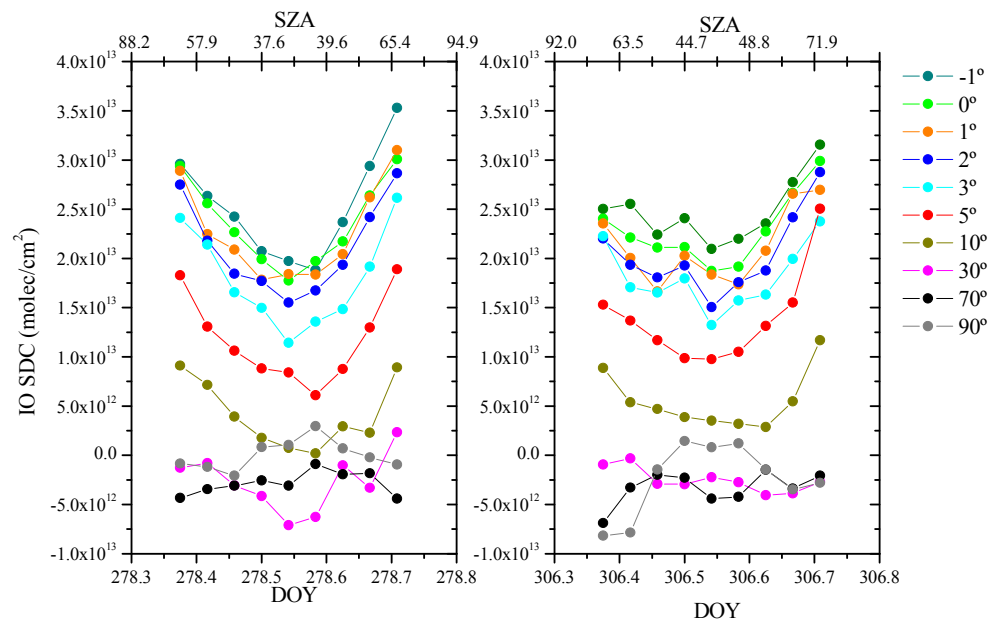
Fig. 4. Diurnal evolution of IO DSCD for elevation angles from −1˚ (below horizon) to 90˚ (zenith) during clear clean days 278 (5 October) and 306 (2 November).

Title Page

Abstract | Introduction

Conclusions | References

Tables | Figures

|◄ | ►|

◄ | ►

Back | Close

Full Screen / Esc

Printer-friendly Version

Interactive Discussion
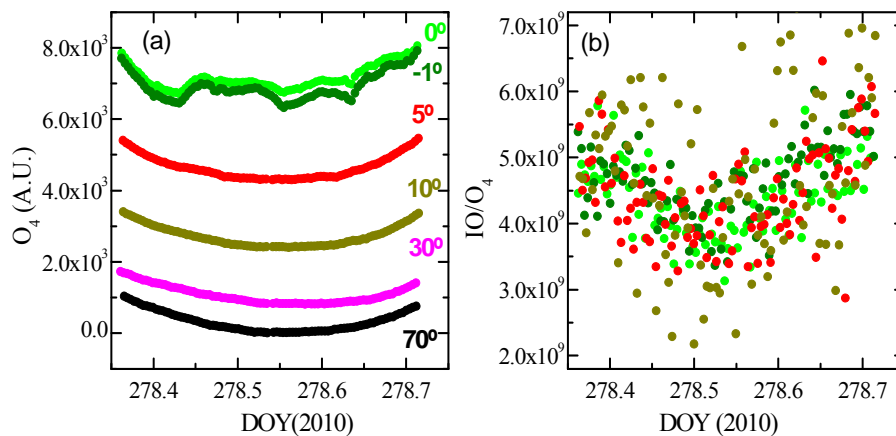
Fig. 5. (a) O_4 diurnal variation on day 278/2010 for a set of elevation angles. **(b)** IO/O_4 ratio for the same day.

ACPD

11, 27833–27860, 2011

Iodine monoxide in the north subtropical free troposphere

O. Puentedura et al.

Title Page

Abstract | Introduction

Conclusions | References

Tables | Figures

◀◀ | ▶▶

◀ | ▶

Back | Close

Full Screen / Esc

Printer-friendly Version

Interactive Discussion
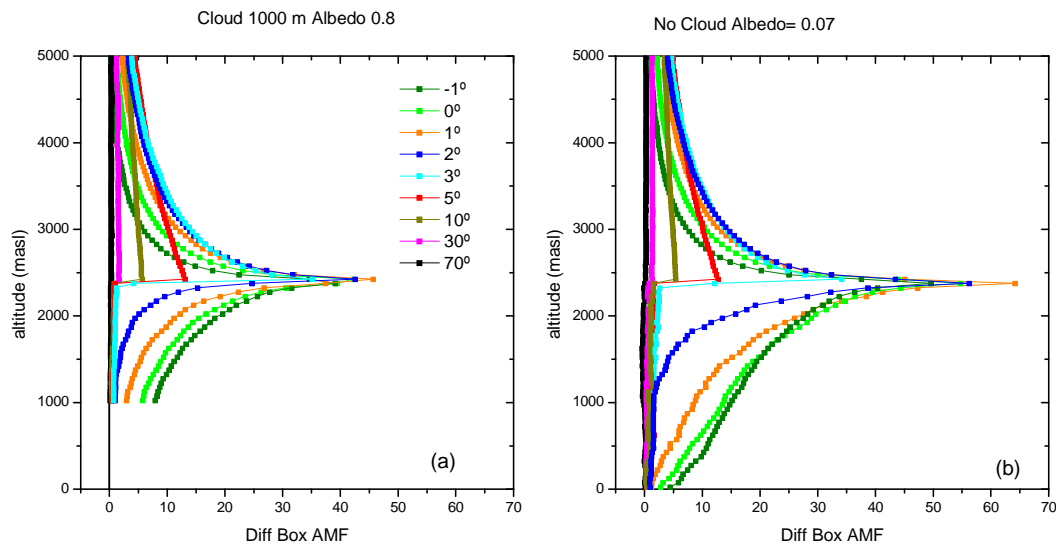
Fig. 6. Differential box-AMF for Izaña at different instrument elevation angles. **(a)** with a cloud at 1000 m a.s.l. and albedo 0.8. **(b)** Without a cloud and albedo 0.07 (see text).
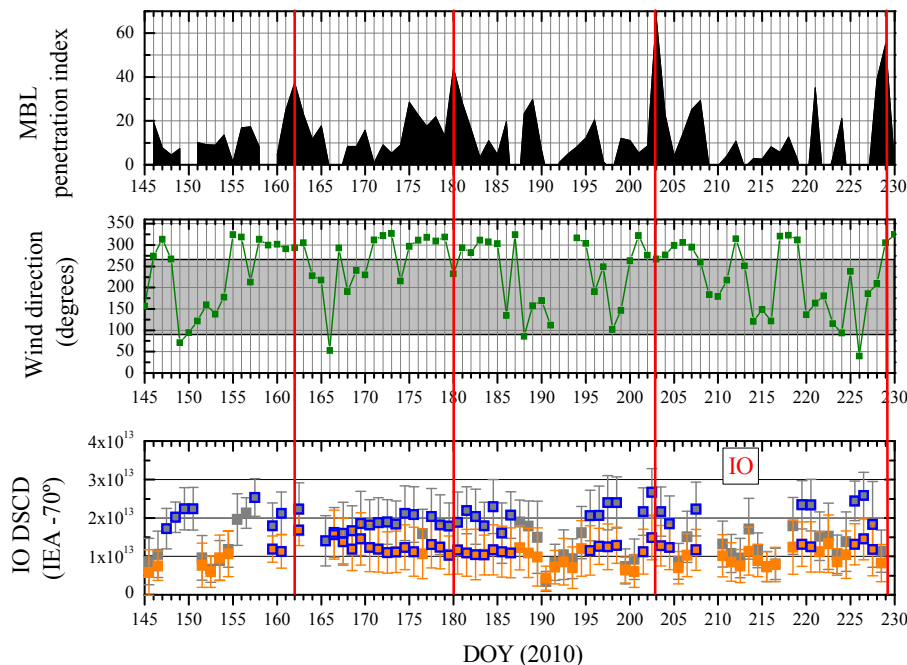
Fig. 7. Upper panel, MBL penetration index for H_2O (see text). Middle panel, wind direction. Bottom panel, in grey: IO DCSD(0°–70°) and in orange: DCSD(5°–70°) data series. Hollow blue are pristine days.

Title Page

Abstract | Introduction

Conclusions | References

Tables | Figures

◄◄ | ►►|

◄ | ►

Back | Close

Full Screen / Esc

Printer-friendly Version

Interactive Discussion
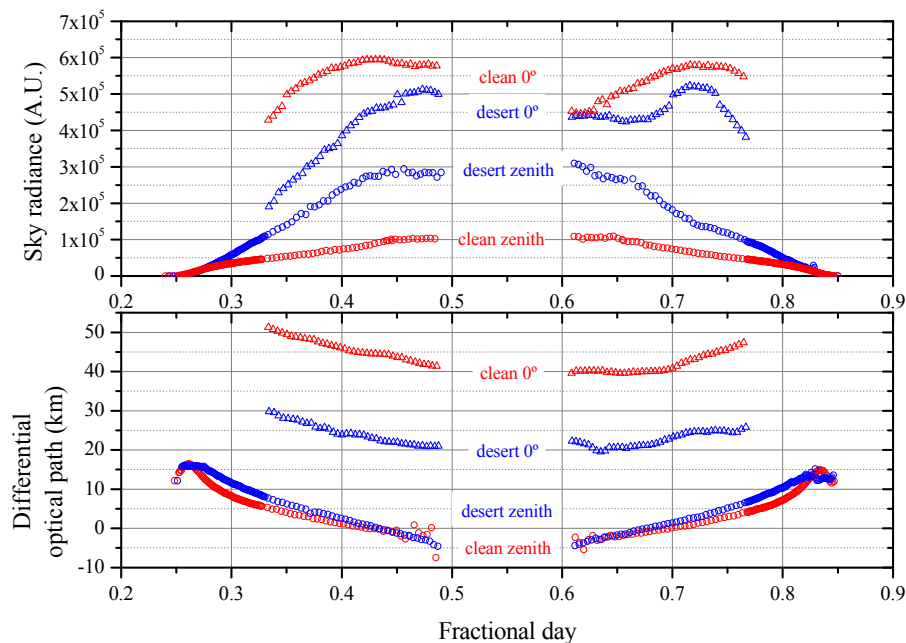
Fig. 8. Upper panel, sky radiance at zenith (circles) and horizon (triangles) for a clean (red) and desert (blue) days. Bottom panel, differential optical path for the same cases as upper panel. Clean is day 181/2010 (30 June). Desert is day 190/2010 (9 July).